Title

Adaptive optics microscopy enhances image quality in deep layers ofCLARITY processed brains of YFP-H mice

Authors

Reinig, Marc
Novak, Samuel
Tao, Xiaodong
et al.

Publication Date

2016

Adaptive optics microscopy enhances image quality in deep layers of CLARITY processed brains of YFP-H mice

Marc R. Reinig[*a], Samuel W. Novack[a], Xiaodong Tao[a], Florian Ermini[a], Laurent A. Bentolila[b], Dustin G. Roberts[b], Allan MacKenzie-Graham[b], S. E. Godshalk[c], M. A. Raven[c], and Joel Kubby[a], [a]W. M. Keck Center for Adaptive Optical Microscopy (CfAOM) at Univ. of California Santa Cruz (United States); [b]Univ. of California, Los Angeles (United States); [c]NRI-MCDB Microscopy Facility, Univ. of California, Santa Barbara (United States)

ABSTRACT

Optical sectioning of biological tissues has become the method of choice for three-dimensional histological analyses. This is particularly important in the brain were neurons can extend processes over large distances and often whole brain tracing of neuronal processes is desirable. To allow deeper optical penetration, which in fixed tissue is limited by scattering and refractive index mismatching, tissue-clearing procedures such as CLARITY have been developed. CLARITY processed brains have a nearly uniform refractive index and three-dimensional reconstructions at cellular resolution have been published. However, when imaging in deep layers at submicron resolution some limitations caused by residual refractive index mismatching become apparent, as the resulting wavefront aberrations distort the microscopic image. The wavefront can be corrected with adaptive optics. Here, we investigate the wavefront aberrations at different depths in CLARITY processed mouse brains and demonstrate the potential of adaptive optics to enable higher resolution and a better signal-to-noise ratio. Our adaptive optics system achieves high-speed measurement and correction of the wavefront with an open-loop control using a wave front sensor and a deformable mirror. Using adaptive optics enhanced microscopy, we demonstrate improved image quality wavefront, point spread function, and signal to noise in the cortex of YFP-H mice.

Keywords: Adaptive Optics, CLARITY, Mouse Brain, Two-photon microscope

1. INTRODUCTION

Our ability to look deep within brain tissue, using fluorescent imaging, is primarily limited by refractive index (RI) inhomogeneities and mismatches. These cause light scattering and distortion of the point-spread function (PSF) and result in reduced intensity, resolution, contrast, and penetration depth. Limitations in the working depth of objective lenses also limit our ability to peer deeply into the structures.

The light scattering qualities of brain tissue comes primarily from high concentrations of lipids. The distortion of the PSF originate from several factors: the RI mismatch between the microscope lens, index matching fluid, coverslip and the bulk RI of the tissue which cause depth dependent spherical aberration; the tilt of these elements and internal tissue structures relative to the lens can cause coma and astigmatism; and inhomogeneities in the RI of the tissue cause further degradation from the resultant higher order aberrations.

At a relatively shallow depth (100μm), in brain tissue, scattering due to lipids becomes significant and, very soon after, no amount of improvement in the PSF can overcome the effects of scattered[1] light in reducing signal intensity, contrast, and resolution. Moving the stimulating light to a longer wavelength allows us to penetrate deeper into the tissue, since scattering is inversely proportional to wavelength. Nevertheless, while using longer wavelength fluorophores or multiphoton excitation[2] has allowed us to go even deeper, scattering still dominates within a few hundred μm. This limits us currently to a penetration of < 1,600μm[3].

In order to image the entire organ, at high resolution, one approach is to slice the brain, image individual slices and then recombine the images. This process is complicated by the physical damage from the slicing, and the fact that the deeper parts of each slice have reduced intensity, resolution, and contrast due to scattering, and aberrations.

* mrr10837@ucsc.edu

Clinical and Translational Neurophotonics; Neural Imaging and Sensing; and Optogenetics and Optical Manipulation, edited by Steen J. Madsen, et. al., Proc. of SPIE Vol. 9690, 969008
 · doi: 10.1117/12.2213283

Fortunately, we can now treat the samples to remove and replace the lipids with a scaffolding of non-scattering polymerized hydrogel using the CLARITY[4,5] technique. This yields an entire organ with the scattering lipids removed allowing us to image fluorophores deep into the almost transparent structure, without the physical damage caused by sectioning, and with the PSF only affected by the residual spherical, coma, astigmatism, and higher order aberrations. However, there are still RI mismatches between the cleared organ and the lens both with CLARITY and other clearing protocols. This leads to spherical aberration which increasingly degrades imaging at deeper depths[6].

A number of techniques have been used to correct for spherical aberrations. Many objective lenses have correction collars that can correct a limited amount of spherical aberration. However, they must be manually adjusted iteratively with the focus control to give the best correction and often cannot correct over the long working distance required for deep imaging. A more sophisticated approach to correct sphere has been to synchronize a motorized correction collar with the stage height controller, but this does not compensate for the collar's limited range. Additionally, some manufacturers have designed lenses specifically to match the index of a certain clearing protocol (see Table 1). These lenses are only corrected for a specific clearing agent and introduce spherical aberrations when used with other agents. Another approach is the use of adaptive optics (AO) to remove the spherical aberrations[7,8]. AO systems can also remove spherical aberration and the correct focal adjustment can be automatically applied without manual intervention. Unfortunately, after the spherical aberration is removed by any of the above means, the residual aberrations remain, including astigmatism, coma, and higher order aberrations, which will still degrade the PSF. These can only be removed by an AO system.

Table 1: Some objectives customized for clearing methods[6].

Model (manufacturer)	Numerical aperture	Clearing agent or immersion medium	Working distance	Refractive index range
HC FLUOTAR L 25×/1.00 IMM (n_e = 1.457) motCORR VISIR	1.0	CLARITY	6 mm	1.45
10× UIS2-XLPLN10XSVMP (Olympus)	0.6	CLARITY, glycerol, Scaleview-A2, SeeDB, water	8 mm	1.33–1.52
25× UIS2-XLSLPLN25XGMP	1.0	Glycerol, CLARITY,	8 mm	1.41–1.52
LSFM Clearing 20×/1.0 (Zeiss)	1.0	CLARITY, CUBIC,	5.6 mm	1.45 ± 0.03
LD Plan-Apochromat 20×/1.0 (Zeiss)	1.0	Scale	5.6 mm	1.38 ± 0.03
EC Plan-NEOFLUAR 5×/0.16 (Zeiss)	0.16	CLARITY, CUBIC,	5.6 mm	1.45

In this paper, we characterize the impact of an AO system on CLARITY brain imaging, when used to remove aberrations beyond simply sphere. To determine the effect of wavefront aberrations on the imaging of the CLARITY brain, we compared images made at various tissue depths with and without AO correction.

2. MATERIALS AND METHODS

2.1 Wavefront metrics

In order to provide an objective measure of a system's performance in imaging we use the Strehl ratio. This is the ratio of a system 's actual PSF to its theoretical diffraction limited PSF in the absence of aberrations[9]. Systems with Strehl ratios of less than 0.3 can be considered poorly corrected, whereas Systems with Strehl ratios above 0.8 are considered well corrected. All aberrations contribute a Root Mean Square (RMS) error, which degrades the wavefront; consequently, we also use the total RMS wavefront error as a metric in our analysis.

We report Zernike single-index orders in Noll form as shown in Table 2. Only the first 22 Zernike modes are reported in our calculations, since those of higher order do not contribute to a significant amount of RMS wavefront error. Zernike orders 1 to 4 (piston, tip, tilt, and focus) are ignored since they are not aberrations but movements of the focal point in X, Y, and Z.

Table 2: Zernike aberrations in Noll single index order.

Index	Zernike
1	Piston
2	Tip
3	Tilt
4	Defocus
5	Oblique astigmatism
6	Vertical astigmatism
7	Vertical coma
8	Horizontal coma
9	Vertical trefoil
10	Oblique trefoil
11	Primary spherical

2.2 Two-photon AO microscope

A two-photon microscope[10, 11] was modified to include an adaptive optics system with an open-loop control system. Figure 1 shows the layout of the system. Two photon excitation is generated by a tunable (680-1080 nm) mode locked Ti:Sapphire laser (140 fs, 80 MHz, Chameleon Ultra II, Coherent) the intensity of which is modulated by an electro-optic modulator (model 350- 80LA, Conoptics Inc.). A 25X water immersion objective with a numerical aperture of 1.05 was used (XLPlan N, Olympus Microscope, Center Valley, PA) for imaging. The photomultiplier tube (PMT) (H7422-20, Hamamatsu) is configured in a non-descanned mode, and collects the emitted light during imaging. To correct wavefront aberrations, a deformable mirror (DM) (Boston Micromachines) with 140 actuators and 3.5μm of stroke is used.in conjunction with a 44x44-lenslet array in a Shack-Hartmann wavefront sensor (SHWS). The SHWS collects fully descanned light during wavefront measurement from selected points in the imaging plane. (For more complete details of the system, see reference [10] and [11] above). Imaging was done using a wavelength of 900nm for two-photon excitation of the fluorophores. Wavefront measurements were made at a wavelength of 515nm.

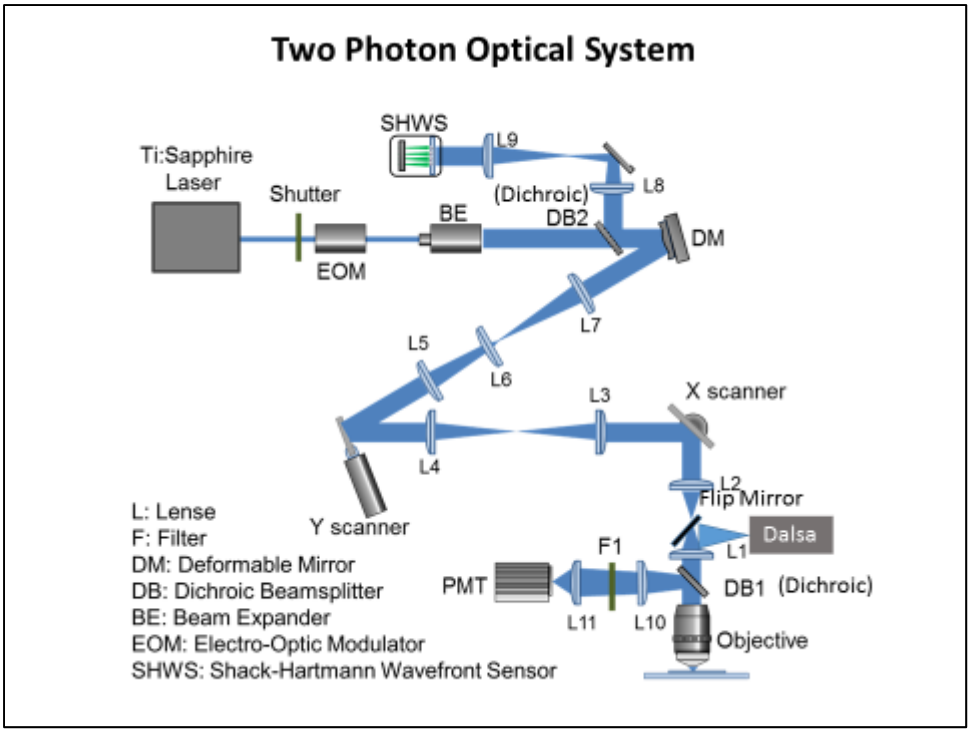

Figure 1: Two-Photon AO Setup

2.3 CLARITY mouse brains

Two different samples of optically cleared mouse brains were used in this study. M. Raven, UCSB, provided a whole optically cleared mouse brain labelled for the astrocytic marker glial fibrillary acidic protein (GFAP).

A dissected section of optically cleared brain tissue from a Thy1-YFP mouse (Jackson Laboratories, Bar Harbor, ME) was provided by courtesy of Laurent Bentolila, UCLA). This sample was enclosed in a custom slide chamber and immersed in FocusClear media (CelExplorer, Hsinchu, Taiwan).

2.4 Measurement methods

To determine the effect of wavefront aberrations on the imaging of the CLARITY brain, we compared images made at various depths with and without AO correction.

2.5 Making the wavefront measurements

Images from the SHWF sensor were used to determine an unaberrated reference wavefront. The reference images were taken from a 100nm fluorescent bead on a slide under a #1.5 (170µm) coverslip mounted with Vectashield (Vector Laboratories). This became the reference wavefront representing an unaberrated wavefront. The bead slide was then replaced with the brain slide for imaging and wavefront measurements were made at various depths. The first 22 Zernike aberrations were measured, and the wavefront RMS wavefront error and Strehl ratio were determined. Excitation wavelength was centered at 900nm. Emission wavelength was centered at 515nm. Wavefronts were measured at the emission wavelength and the compensation during imaging was applied to the 900nm excitation after compensation for dispersion.

Aberrations in a CLARITY whole brain sample were measured from the surface to a depth of 1,500µm in increments of 50µm. No coverslip was used and the lens (a water immersion lens) was immersed directly in a CLARITY solution. This mismatch in RI caused some spherical aberration. At each stage, we measured and analyzed the wavefront for aberrations. For each stack of CLARITY micrographs, the first 22 Zernike aberrations were determined from a section

near the middle of the stack and used to calculate the corresponding voltages required to produce a complimentary phase shift in the deformable mirror.

Imaging of the brain sections was accomplished at a depth of 500µm. Here, the brain was enclosed in a custom holder under a standard 0.17mm coverslip. Water was used with the water immersion lens (see Figure 2).

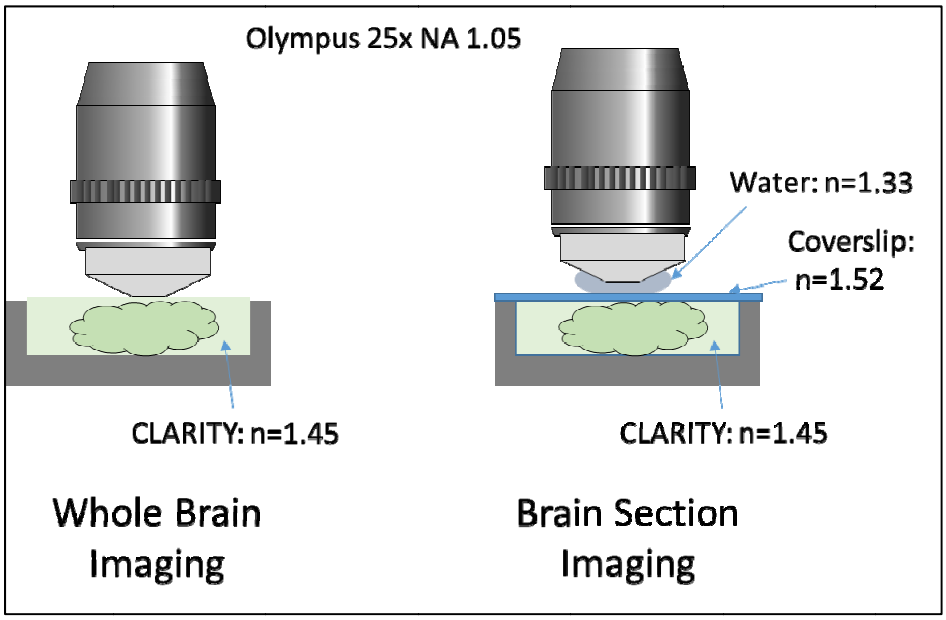

Figure 2: Imaging whole brains and brain sections

3. RESULTS

We present two analyses here. The first is a summary of the aberrations at in our deep scan to 1,500µm in 50µm steps. Here we focused on the comparative amount of spherical aberration to other aberrations. Spherical aberrations can be removed by a collar on the objective or by an AO system, whereas the other non-spherical aberrations can only be removed by an AO system. The second analysis was of the effect on imaging of removing only spherical aberrations compared to removing all aberrations. This was performed at a depth of 500µm. We measured the wavefront and calculated RMS wavefront error and Strehl ratio in a variety of locations on the sample. Imaging was done without AO, with only sphere compensated by AO, and with all aberrations compensated by AO.

3.1 Comparing aberrations from 0 to 1,500µm

To examine the effects of AO correction at different focal depths, we examined a whole CLARITY treated mouse brain immunostained for the astrocytic marker GFAP, provided by M. Raven, UCSB. At 1,500µm depth, we measured the wavefront and calculated RMS wavefront error and the Strehl ratio (Figure 3). As expected, we found a decreased Strehl ratio and worsened RMS wavefront error values as the depth of the measurements increased.

Imaging with AO wavefront correction resulted in an increase of the signal-to-noise ratio from 40 to 250% (Figure 3). AO correction revealed fine details of small astrocytic processes were observable. Astrocytes are involved in regulating neural signaling and tissue homeostasis and are important signal mediators between the brain and the vasculature. Most of these processes are performed though contact with astrocytic end feet, a process that could be studied in greater detail with the help of AO.

Figure 4 and Figure 5 show the increasing contribution of the non-spherical aberrations to the RMS wavefront error and reduction in the Strehl ratio as the depth increases. At a depth of 1,500µm, the RMS wavefront error contributed by non-spherical aberrations is approximately equal to that of the spherical aberration.

In Figure 4 it is important to note that horizontal coma is not decreasing as depth increases, it is increasing in a negative direction and adding RMS wavefront error to the wavefront.

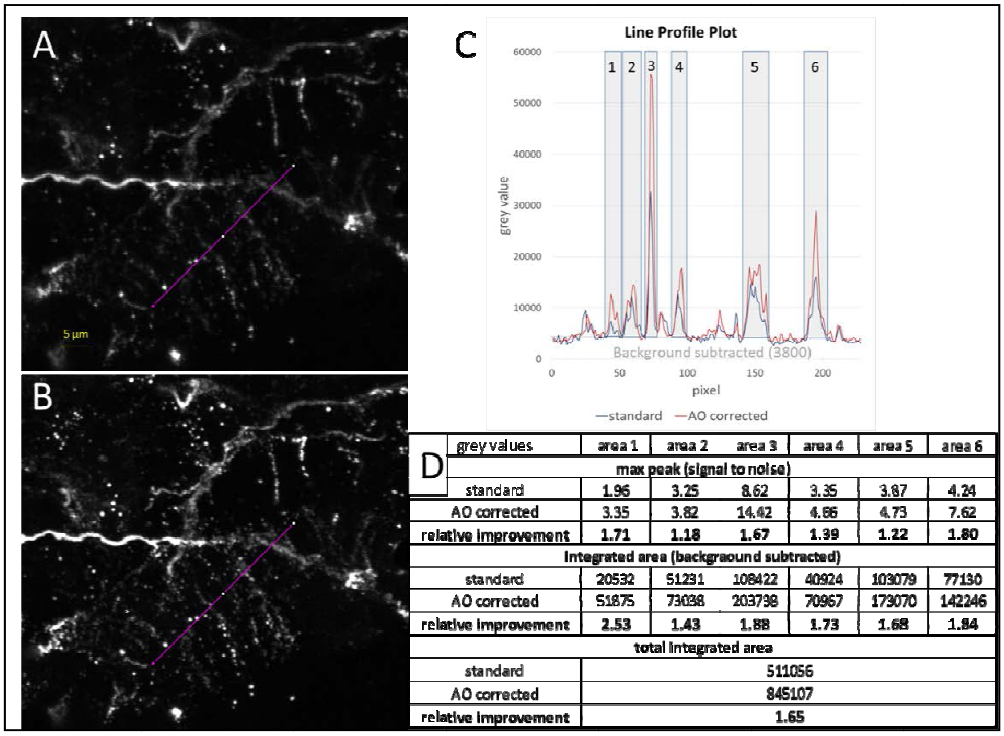

D

grey values	area 1	area 2	area 3	area 4	area 5	area 6
max peak (signal to noise)						
standard	1.96	3.25	8.62	3.35	3.87	4.24
AO corrected	3.35	3.82	14.42	4.66	4.73	7.62
relative improvement	1.71	1.18	1.67	1.39	1.22	1.80
integrated area (backgraound subtracted)						
standard	20532	51231	108422	40924	103079	77130
AO corrected	51875	73038	203798	70967	173070	142246
relative improvement	2.53	1.43	1.88	1.73	1.68	1.84

total integrated area	
standard	511056
AO corrected	845107
relative improvement	1.65

Figure 3: Two-photon image stacks (12.3µm thick) (Z step size 0.8µm) of astrocytes at 1,500µm depth in a CLARITY mouse brain. **A**: uncorrected maximal projection; **B**: AO corrected maximal projection; **C**: Line profile plot of the magenta lines in A-B with peaks highlighted as areas 1to 6; **D**: data analysis of the line profile plot and areas 1 to 6.

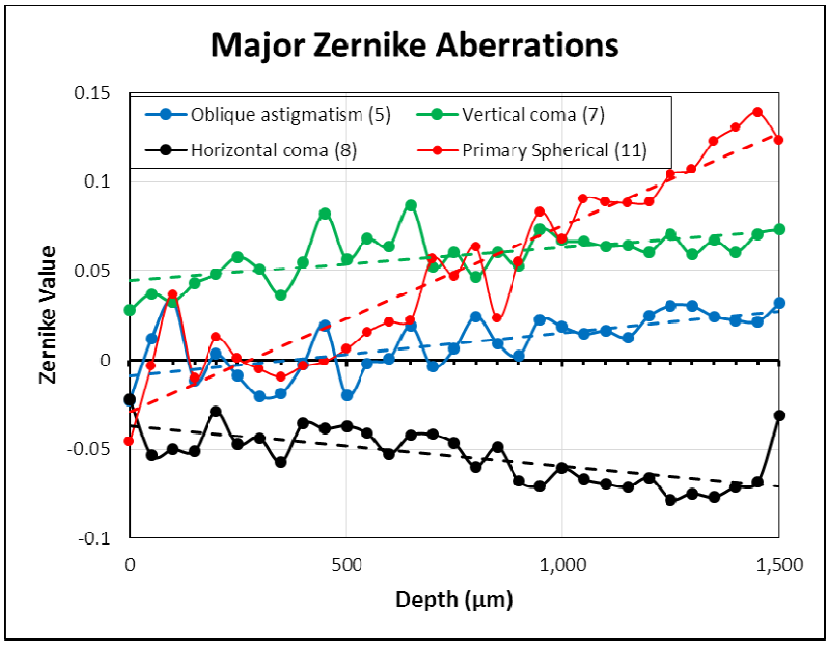

Figure 4: Major Zernike aberrations increase as depth increases. NB: horizontal coma does not decrease with depth; it is increasing in a negative direction and adding RMS error to the wavefront.

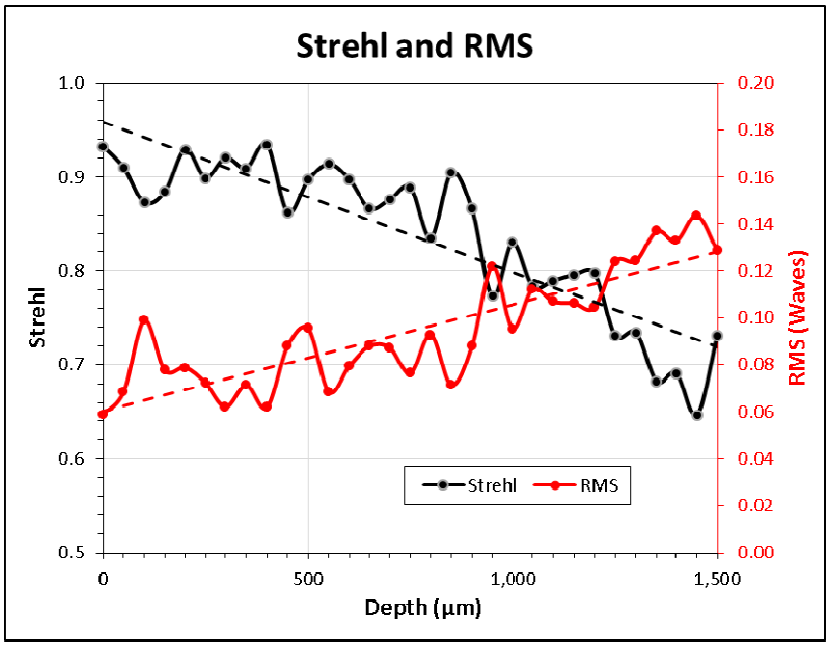

Figure 5: Decreasing Strehl ratio and increasing RMS wavefront error vs. depth in the optically cleared mouse brain indicate the diminished wavefront quality as focal depth increases.

3.2 Analysis of aberrations at 500µm depth

The relationships between the different aberrating components were determined by acquiring images and corresponding wavefront measurements under three conditions: (1) without AO; (2) with only sphere compensated by AO; and (3) with all aberrations corrected with AO.

Stacks were collected at a depth of approximately 500µm below the coverslip, where features were readily observable without AO but were obviously improved with the appropriate AO correction. Figure 6 and Figure 7 illustrate the improved resolution and signal-to-noise that upon correction for sphere and the even greater correction achieved when all Zernike modes are considered for the wavefront correction. Figure 8 clearly shows that the amount of cumulative RMS wavefront error generated by non-spherical aberrations is significant (Sphere is index 11 and has a value approximately of 0.1)

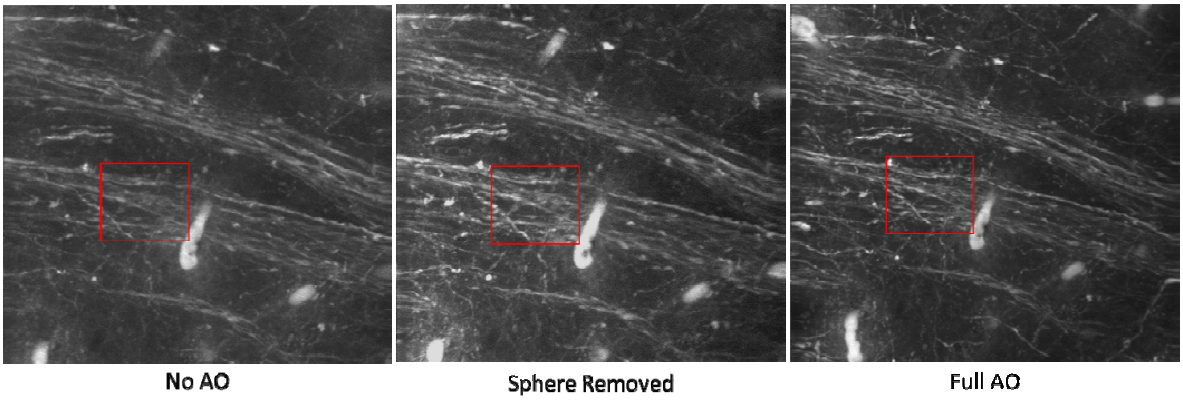

Figure 6: Brain slice position 1. Neurite bundle at a depth of 500µ. The field of view is 85µm x 85µm and is a maximal Z projection of 19 sections spaced at 1.0µm intervals. The inset is shown in Figure 7 below.

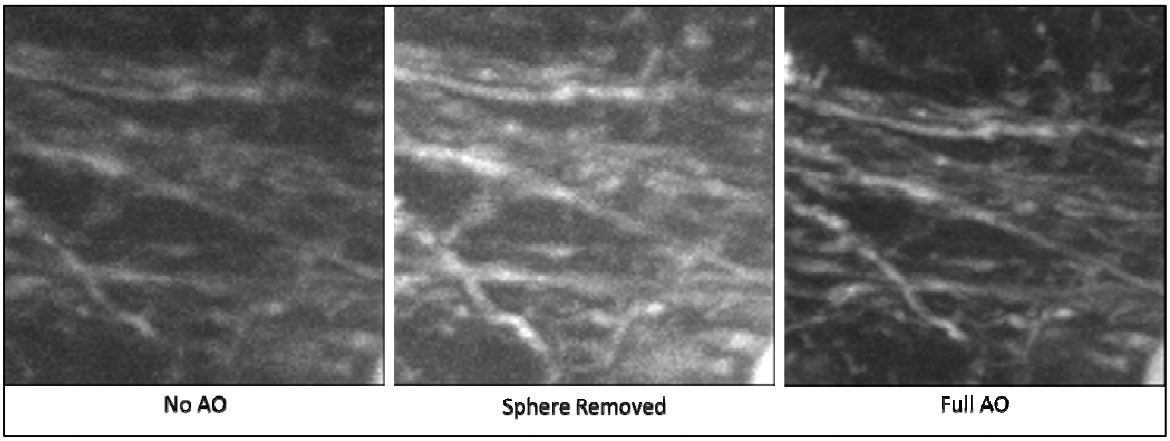

Figure 7: Enlarged image from inset above. The brightness difference of the "Sphere Removed" due to photo bleaching of the fluorophores as it was taken last and had a lower signal-to-noise ratio as a result.

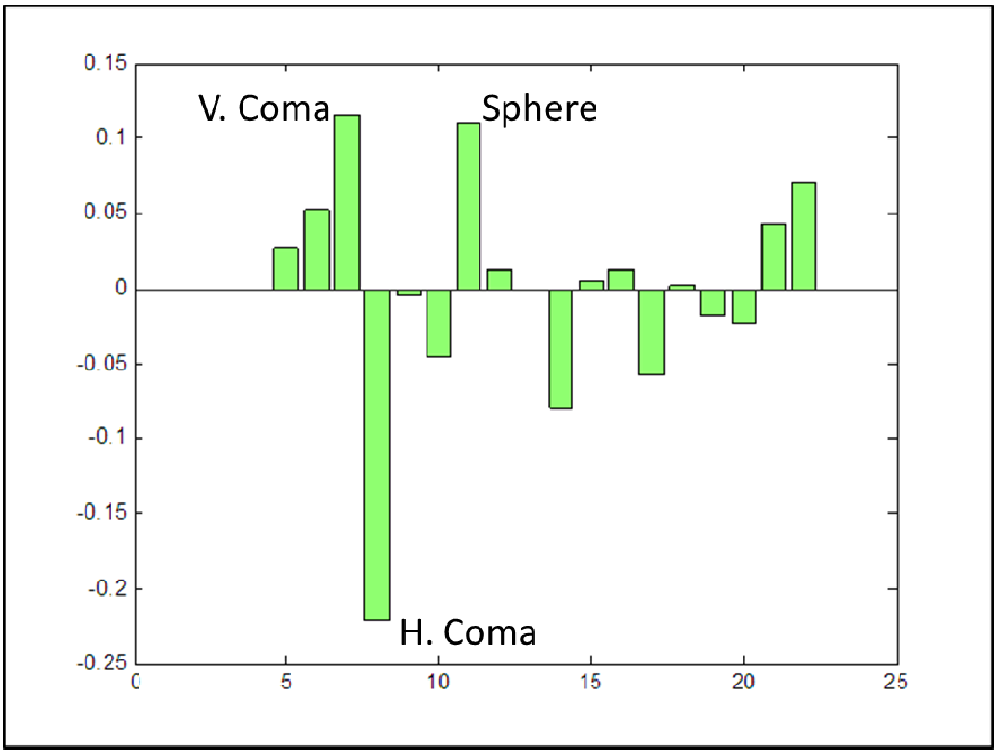

Figure 8: Brain slice position 1. Zernike modes (waves) (in Noll order) of the neurite bundle wavefront prior to AO correction (piston, tip/tilt, focus removed) (Sphere is index 11, at approximately 0.1).

It can be seen in Figure 9 shows images at position 2 at a depth of 500µm, both with and without AO compensation. It can be seen in Figure 10 that even with AO compensation there are still significant residual aberrations. These prevent the images with AO correction from achieving maximum enhancement and resolution. This shortcoming in our compensation is due partially to a limitation in our open-loop control system where we cannot sense or compensate adequately in the presence of large aberrations and partially due to the effects of dispersion between our excitation wavelength (900nm) and our wavefront measurement wavelength (515nm). We are addressing this by optimizing our open-loop algorithm, incorporating an optional closed-loop mode, which has proven capable of reducing residual errors to a minimum, and compensating for the effects of dispersion. All of the residual Zernike values are below 0.1 and most are below 0.05. The RMS wavefront error has been reduced by a factor of three (from 0.26 to 0.9) at a depth of 500µm. Additionally, we have been able to significantly increase the Strehl ratio from 0.22 (poorly corrected) to 0.85 (well corrected).

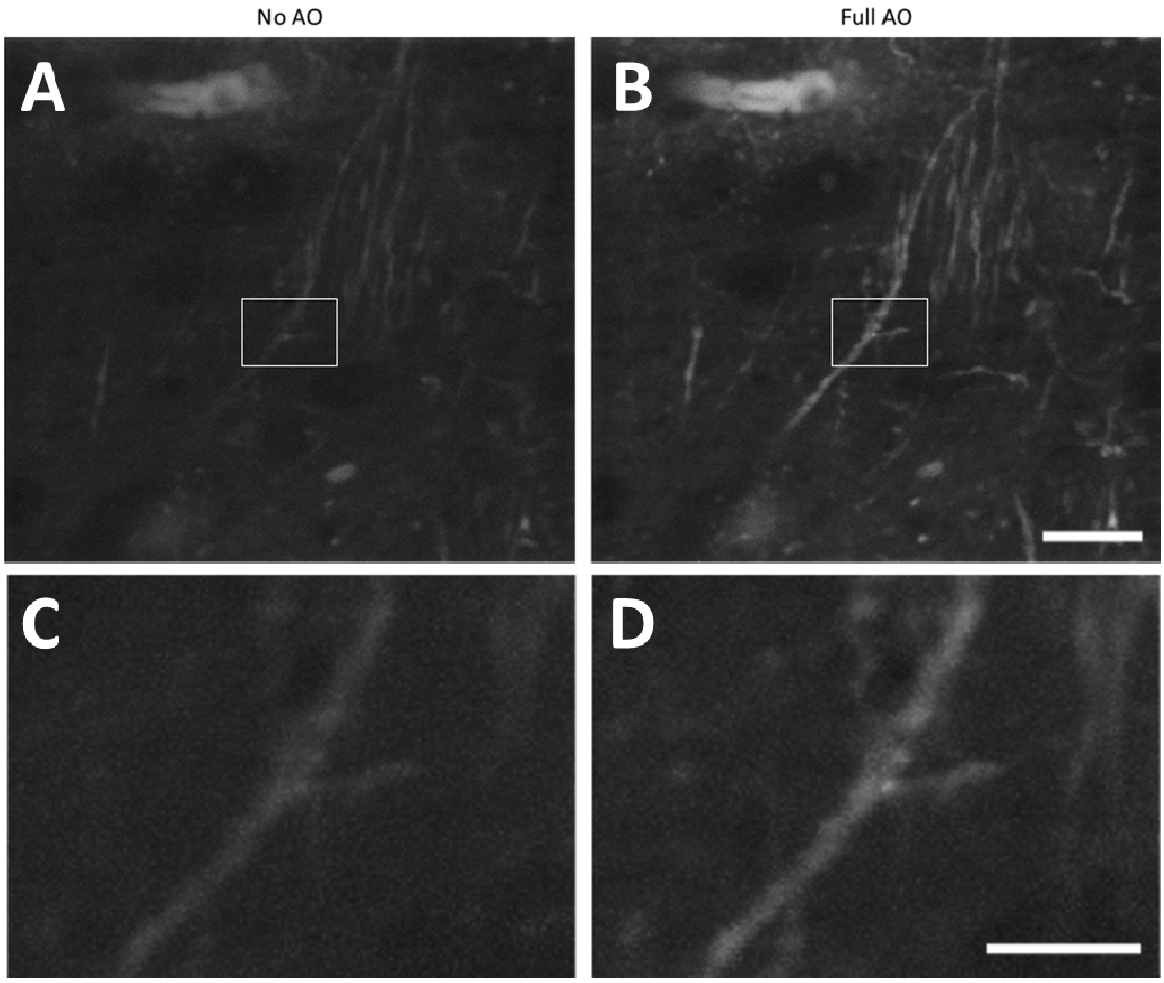

Figure 9: Brain slice position 2. A dendritic segment with dendritic spines is centered in the field of view. Field of view is 55µm x 55µm maximal Z-projection of 20 sections at 500nm intervals. Scale bar is 10µm. **A**: without AO. **B**: with AO. The insets, **C** and **D**, show fine structures are more readily resolved after AO correction. Scale bar is 2µm.

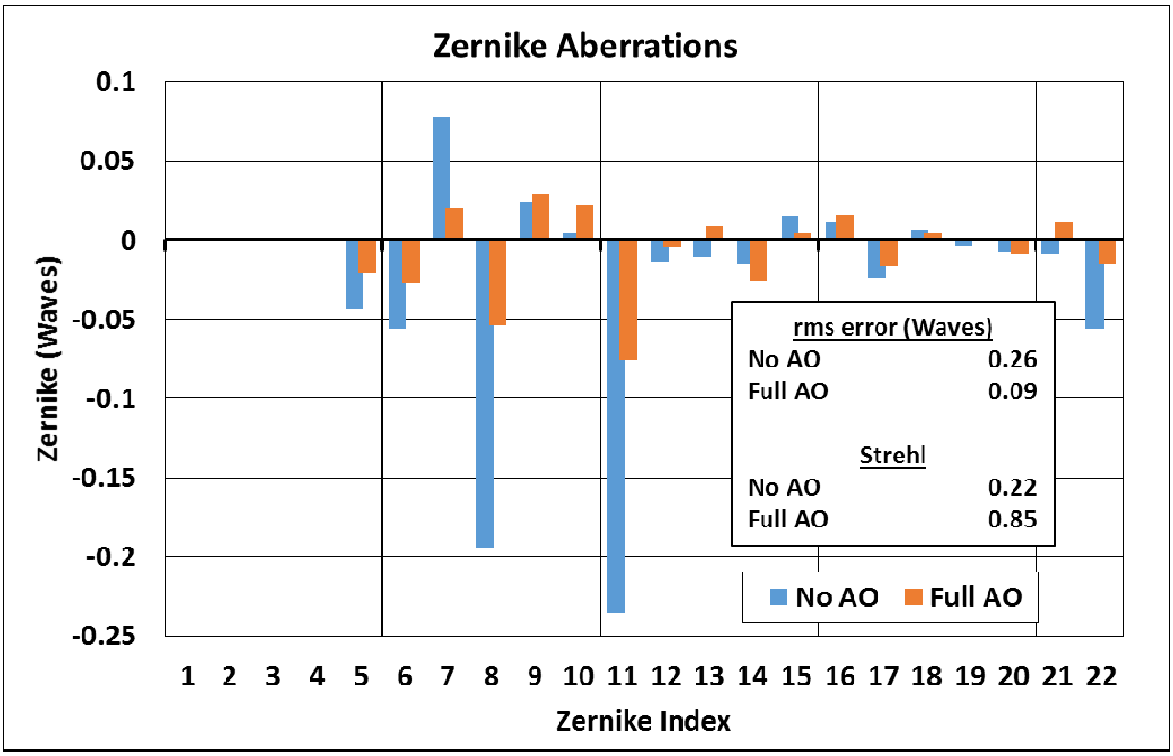

Figure 10: Zernike modes of the wavefront aberrations for the images in Figure 9, illustrating the improved quality of the wavefront after AO correction. Shown before and after AO compensation

4. CONCLUSIONS

CLARITY brains allow examination of deep neurological structures without the degrading effects of scattering found in uncleared brains. However, refractive aberrations still degrade the quality of the image as we peer deeper into the structure. Objective lenses designed for specific clearing agents can minimize spherical aberrations. However, they still introduce spherical aberrations when used with other clearing agents. Microscope objective collars can be adjusted to remove the spherical aberration. In both of these cases, spherical aberrations increase with depth and the objective collar or AO can compensate for it. However, other accumulated aberrations also increase with depth and cannot be removed without a higher order AO system. We have analyzed the increase of aberrations with depth and calculated the impact on the Strehl ratio and RMS wavefront error, as well as image quality, at various depths. This has been verified on CLARITY mouse brains and we have been able to reduce the RMS wavefront error by a factor of three from 0.9 to 0.26 at a depth of 500μm. We have been able to significantly increase the Strehl ratio from 0.22 (poorly corrected) to 0.85 (well corrected) at the same depth. As we probe deeper into CLARITY brains, refractive aberrations other than sphere will require the use of AO to allow us to image structures at the diffraction limit of our system.

ACKNOWLEDGEMENTS

The results presented herein were obtained at the W.M. Keck Center for Adaptive Optical Microscopy (CfAOM) at University of California Santa Cruz. The CfAOM was made possible by the generous financial support of the W.M. Keck Foundation. This material is based upon work supported by the UC Office of the President for the UC Work Group for Adaptive Optics in Biological Imaging, by the Multicampus Research Programs and Initiatives (MRPI), Grant #MR-15-327968. This material is also based upon work supported by the National Science Foundation under Grant. Numbers 1353461 & 1429810. Any opinions, findings, and conclusions or recommendations expressed in this material are those of the authors and do not necessarily reflect the views of the National Science Foundation.

REFERENCES

[1] Aime, C.., Soummer, R., "The Usefulness and Limits of Coronagraphy in the Presence of Pinned Speckles," Astrophys. J. **612**(1), L85–L88 (2004).

[2] Denk, W., Strickler, J. H.., Webb, W. W., "Two-photon laser scanning fluorescence microscopy.," Science **248**(4951), 73–76 (1990).

[3] Cheng, L.-C., Horton, N. G., Wang, K., Chen, S.-J.., Xu, C., "Measurements of multiphoton action cross sections for multiphoton microscopy.," Biomed. Opt. Express **5**(10), 3427–3433, Optical Society of America (2014).

[4] Chung, K., Wallace, J., Kim, S.-Y., Kalyanasundaram, S., Andalman, A. S., Davidson, T. J., Mirzabekov, J. J., Zalocusky, K. A., Mattis, J., et al., "Structural and molecular interrogation of intact biological systems.," Nature **497**(7449), 332–337, Nature Publishing Group, a division of Macmillan Publishers Limited. All Rights Reserved. (2013).

[5] Tomer, R., Ye, L., Hsueh, B.., Deisseroth, K., "Advanced CLARITY for rapid and high-resolution imaging of intact tissues.," Nat. Protoc. **9**(7), 1682–1697 (2014).

[6] Marx, V., "Microscopy: seeing through tissue," Nat. Methods **11**(12), 1209–1214 (2014).

[7] Kner, P., Sedat, J. W., Agard, D. A.., Kam, Z., "High-resolution wide-field microscopy with adaptive optics for spherical aberration correction and motionless focusing.," J. Microsc. **237**(2), 136–147 (2010).

[8] Tsai, P. S., Migliori, B., Campbell, K., Kim, T. N., Kam, Z., Groisman, A.., Kleinfeld, D., "Spherical aberration correction in nonlinear microscopy and optical ablation using a transparent deformable membrane," Appl. Phys. Lett. **91**(19), 191102, AIP Publishing (2007).

[9] Hardy, J. W., [Adaptive optics for astronomical telescopes], Phys. Today **53**(4), Oxford University Press (1998).

[10] Tao, X., Norton, A., Kissel, M., Azucena, O.., Kubby, J., "Adaptive optics two photon microscopy with direct wavefront sensing using autofluorescent guide-stars," Proc. SPIE Vol. 8978, T. G. Bifano, J. Kubby, and S. Gigan, Eds., 89780D (2014).

[11] Tao, X., Norton, A., Kissel, M., Azucena, O.., Kubby, J., "Adaptive optical two-photon microscopy using autofluorescent guide stars.," Opt. Lett. **38**(23), 5075–5078 (2013).